Comput Mech
DOI 10.1007/s00466-012-0700-3

ORIGINAL PAPER

Comparison of the performance of SSPH and MLS basis functions for two-dimensional linear elastostatics problems including quasistatic crack propagation

C. L. Tsai · Y. L. Guan · R. C. Batra · D. C. Ohanehi · J. G. Dillard · E. Nicoli · D. A. Dillard

Received: 16 August 2011 / Accepted: 4 March 2012

Abstract We use symmetric smoothed particle hydrodynamics (SSPH) and moving least squares (MLS) basis functions to analyze six linear elastostatics problems by first deriving their Petrov-Galerkin approximations. With SSPH basis functions one can approximate the trial solution and its derivatives by using different basis functions whereas with MLS basis functions the derivatives of the trial solution involve derivatives of the basis functions used to approximate the trial solution. The class of allowable kernel functions for SSPH basis functions includes constant functions which are excluded in MLS basis functions if derivatives of the trial solution are also to be approximated. We compare results for different choices of weight functions, size of the compact support of the weight function, order of complete polynomials, and number of particles in the problem domain. The two basis functions are also used to analyze crack initiation and propagation in plane stress mode-I deformations of a plate made of a linear elastic isotropic and homogeneous material with particular emphasis on the computation of the T-stress. The crack trajectories predicted by using the two basis functions agree well with those found experimentally.

Keywords Meshless method · Symmetric smoothed particle hydrodynamics (SSPH) basis functions · Moving least squares (MLS) basis functions · Crack propagation

C. L. Tsai · Y. L. Guan · R. C. Batra (✉) · D. C. Ohanehi · E. Nicoli · D. A. Dillard
Department of Engineering Science and Mechanics, M/C 0219, Virginia Polytechnic Institute and State University, Blacksburg, VA 24061, USA
e-mail: rbatra@vt.edu

J. G. Dillard
Department of Chemistry, M/C0212, Virginia Polytechnic Institute and State University, Blacksburg, VA 24061, USA

1 Introduction

One of the important issues in numerical methods of finding an approximate solution of an initial-boundary-value problem (IBVP) is the choice of basis functions. In the finite element method (FEM) one generally uses complete polynomials defined piecewise on the domain of study, and can improve the accuracy of the computed solution either by increasing the number of finite elements or by increasing the degree of complete polynomials. Basis functions in meshless methods of finding an approximate solution of an IBVP include those derived by the smoothed particle hydrodynamics (SPH) method [1], the moving least squares (MLS) approximation [2], the reproducing kernel particle method (RKPM) [3], the corrected smoothed particle hydrodynamics (CSPH) method, the radial basis functions (RBFs) [4], the partition of unity basis functions [5], the modified smoothed particle hydrodynamics method (MSPH) [6,7] and the symmetric smoothed particle hydrodynamics (SSPH) method. Zhang and Batra [8,9] have discussed relations among the SSPH and other basis functions and also with the FE basis functions. Whereas the FE basis functions satisfy the Kronecker delta property, most other basis functions do not. Ideally one should solve several IBVPs using different basis functions to compare their relative performance in terms of the computational effort, the rate of convergence and the accuracy of computed solutions. Here we do so for two basis functions, namely the SSPH and the MLS, and analyze static problems primarily because lessons learned from them can be applied to solving IBVPs within each time step. The choice of basis functions is dictated by the observation that the MLS basis functions have been widely used to analyze IBVPs and the SSPH basis functions the least. The choice of BVPs is guided by our eventual goal of analyzing the failure of adhesively bonded joints. For two problems we also compare the

Journal: 466 MS: 0700 ☐ TYPESET ☐ DISK ☐ LE ☐ CP Disp.:2012/3/24 Pages: 16 Layout: Large

performance of the MLS and the SSPH basis function with that of the pseudo-derivatives proposed by Krongauz and Belytschko [10]. Like the SSPH basis functions, the pseudo-derivatives method employs different basis functions for the trial solution and its derivatives.

Whereas analytical results for error bounds are available in the literature for approximate solutions of linear BVPs studied by the FEM, such results are scarce for solutions derived by a meshless method. In general, the computational effort required to increase the degree of complete polynomials in the MLS basis functions for BVPs involving 2nd order spatial derivatives of the unknown function is more than that required in the SSPH basis functions. A goal of the present work is to determine, through numerical experiments, if the rate of convergence of the numerical solution increases with an increase in the degree of complete polynomials. We refer the reader to two books [11,12] on meshless methods for the background material.

The paper is organized as follows. In Sects. 2 and 3 we briefly review SSPH and MLS basis functions and provide a weak formulation of a two-dimensional BVP in elastostatics. In Sect. 4 we use these two basis functions to numerically solve the cylindrical bending of a cantilever plate and compare the two numerical solutions with the analytical solution of the problem. We thus find the optimum order of complete polynomials used to generate basis functions, the choice of the weight function, and the radius of the compact support of the weight function. We use the optimum values of these variables and the two basis functions to find the stress concentration factor around a hole in a plate loaded in tension. The stress intensity factor near a crack tip in a plate with either one crack at the centroid or two cracks at the centers of vertical edges is studied in Sect. 5. In Sect. 6 we show that crack paths computed in an asymmetric prenotched plate by using the SSPH and the MLS basis functions agree well with those observed experimentally. Conclusions of the work are briefly summarized in Sect. 8.

2 Basis functions for meshless methods considered in this work

2.1 Symmetric smoothed particle hydrodynamics (SSPH) basis functions

The value of function f(**x**) having continuous derivatives up to (m + 1) order at a point $\boldsymbol{\xi} = (\xi_1, \xi_2, \xi_3)$ in the domain of definition of f(**x**) can be approximated in terms of the value of f(**x**) and of its derivatives at the point $\mathbf{x} = (x_1, x_2, x_3)$ by the following finite Taylor series:

$$\mathrm{f}(\boldsymbol{\xi}) = \sum_{k=0}^{m} \frac{1}{k!} \left[(\xi_1 - x_1) \frac{\partial}{\partial x_1} + (\xi_2 - x_2) \frac{\partial}{\partial x_2} + (\xi_3 - x_3) \frac{\partial}{\partial x_3} \right]^k \mathrm{f}(\mathbf{x}) . \tag{2.1}$$

Eq. (2.1) can be viewed as expressing f($\boldsymbol{\xi}$) in terms of the complete polynomial of order m in $\boldsymbol{\xi}$. We set $m = 2$, and rewrite Eq. (2.1) in terms of matrices $\mathbf{P}(\boldsymbol{\xi}, \mathbf{x})$ and $\mathbf{Q}(\mathbf{x})$ as

$$\mathrm{f}(\boldsymbol{\xi}) = \mathbf{P}(\boldsymbol{\xi}, \mathbf{x}) \mathbf{Q}(\mathbf{x}) , \tag{2.2}$$

where

$$\mathbf{P}(\boldsymbol{\xi}, \mathbf{x}) = [1, \xi_1 - x_1, \xi_2 - x_2, \xi_3 - x_3, (\xi_1 - x_1)^2 , (\xi_2 - x_2)^2 , (\xi_3 - x_3)^2 , (\xi_1 - x_1)(\xi_2 - x_2), (\xi_2 - x_2)(\xi_3 - x_3), (\xi_1 - x_1)(\xi_3 - x_3)],$$

$$\mathbf{Q}(\mathbf{x}) = \left[\mathrm{f}(\mathbf{x}) , \frac{\partial}{\partial x_1}\mathrm{f}(\mathbf{x}) , \frac{\partial}{\partial x_2}\mathrm{f}(\mathbf{x}) , \frac{\partial}{\partial x_3}\mathrm{f}(\mathbf{x}) , \frac{1}{2}\frac{\partial^2}{\partial x_1^2}\mathrm{f}(\mathbf{x}) , \frac{1}{2}\frac{\partial^2}{\partial x_2^2}\mathrm{f}(\mathbf{x}) , \frac{1}{2}\frac{\partial^2}{\partial x_3^2}\mathrm{f}(\mathbf{x}) , \frac{\partial^2}{\partial x_1 \partial x_2}\mathrm{f}(\mathbf{x}) , \frac{\partial^2}{\partial x_2 \partial x_3}\mathrm{f}(\mathbf{x}) , \frac{\partial^2}{\partial x_1 \partial x_3}\mathrm{f}(\mathbf{x}) \right] .$$

Elements of matrix $\mathbf{Q}(\mathbf{x})$, i.e., the function as well as the first and the second derivatives of function f(**x**), are unknowns to be found. Elements of matrix $\mathbf{P}(\boldsymbol{\xi}, \mathbf{x})$ are known and are complete polynomials of degree 2. In order to find elements of matrix $\mathbf{Q}(\mathbf{x})$ we post-multiply both sides of Eq. (2.2) with $\mathrm{W}(\boldsymbol{\xi}, \mathbf{x}) \mathbf{P}(\xi, \mathbf{x})^{\mathrm{T}}$ and obtain

$$\mathrm{f}(\boldsymbol{\xi}) \mathrm{W}(\boldsymbol{\xi}, \mathbf{x}) \mathbf{P}(\boldsymbol{\xi}, \mathbf{x})^{\mathrm{T}} = \mathbf{P}(\boldsymbol{\xi}, \mathbf{x}) \mathbf{Q}(\mathbf{x}) \mathrm{W}(\boldsymbol{\xi}, \mathbf{x}) \mathbf{P}(\boldsymbol{\xi}, \mathbf{x})^{\mathrm{T}},$$
$$= \left[\mathbf{P}(\boldsymbol{\xi}, \mathbf{x}) \mathrm{W}(\boldsymbol{\xi}, \mathbf{x}) \mathbf{P}(\boldsymbol{\xi}, \mathbf{x})^{\mathrm{T}} \right] \mathbf{Q}(\mathbf{x}) , \tag{2.3}$$

where $\mathrm{W}(\boldsymbol{\xi}, \mathbf{x})$ is weight function of compact support associated with particle **x**, as shown in Fig. 1. Let there be N(**x**) particles in the compact support of **x**. Eq. (2.3) is evaluated for every particle in the compact support of $\mathrm{W}(\boldsymbol{\xi}, \mathbf{x})$, and summed to obtain

$$\sum_{I=1}^{N(\mathbf{x})} \mathrm{f}\left(\boldsymbol{\xi}^{\mathrm{I}}\right) \mathrm{W}\left(\boldsymbol{\xi}^{\mathrm{I}}, \mathbf{x}\right) \mathbf{P}\left(\boldsymbol{\xi}^{\mathrm{I}}, \mathbf{x}\right)^{\mathrm{T}}$$
$$= \sum_{I=1}^{N(\mathbf{x})} \left[\mathbf{P}(\boldsymbol{\xi}^{\mathrm{I}}, \mathbf{x})^{\mathrm{T}} \mathrm{W}\left(\boldsymbol{\xi}^{\mathrm{I}}, \mathbf{x}\right) \mathbf{P}\left(\boldsymbol{\xi}^{\mathrm{I}}, \mathbf{x}\right) \right] \mathbf{Q}(\mathbf{x}) , \tag{2.4}$$

where $\boldsymbol{\xi}^{\mathrm{I}}$ denotes coordinates of the Ith particle in the compact support of $\mathrm{W}(\boldsymbol{\xi}, \mathbf{x})$. We set

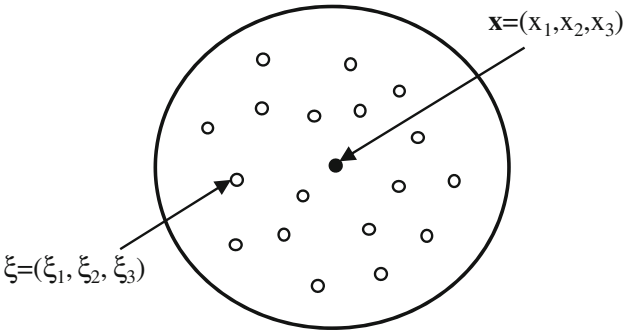

Fig. 1 Distribution of particles in the compact support of $W(\boldsymbol{\xi}, \mathbf{x})$ associated with point $\mathbf{x}$

$$\mathbf{H}(\boldsymbol{\xi}, \mathbf{x}) = \left[\mathbf{P}^{\mathrm{T}}\left(\boldsymbol{\xi}^{1}, \mathbf{x}\right), \mathbf{P}^{\mathrm{T}}\left(\boldsymbol{\xi}^{2}, \mathbf{x}\right), \ldots, \mathbf{P}^{\mathrm{T}}\left(\boldsymbol{\xi}^{\mathrm{N(x)}}, \mathbf{x}\right)\right],$$

$$\mathbf{W}(\boldsymbol{\xi}, \mathbf{x}) = \begin{bmatrix} W\left(\boldsymbol{\xi}^{1}, \mathbf{x}\right) & 0 & \ldots & 0 \\ 0 & W\left(\boldsymbol{\xi}^{2}, \mathbf{x}\right) & \ldots & \vdots \\ \vdots & \vdots & \ddots & 0 \\ 0 & 0 & \ldots & W\left(\boldsymbol{\xi}^{\mathrm{N(x)}}, \mathbf{x}\right) \end{bmatrix},$$

$$\mathbf{F}^{\mathrm{T}}(\boldsymbol{\xi}) = \left[f\left(\boldsymbol{\xi}^{1}\right), f\left(\boldsymbol{\xi}^{2}\right), \ldots, f\left(\boldsymbol{\xi}^{\mathrm{N(x)}}\right)\right].$$

Thus, Eq. (2.4) can be written as

$$\mathbf{H}(\boldsymbol{\xi}, \mathbf{x})\, \mathbf{W}(\boldsymbol{\xi}, \mathbf{x})\, \mathbf{F}(\boldsymbol{\xi}) = \mathbf{H}(\boldsymbol{\xi}, \mathbf{x})\, \mathbf{W}(\boldsymbol{\xi}, \mathbf{x})\, \mathbf{H}^{\mathrm{T}}(\boldsymbol{\xi}, \mathbf{x})\, \mathbf{Q}(\mathbf{x}). \tag{2.5}$$

In Eq. (2.5), values of elements of matrices $\mathbf{H}(\boldsymbol{\xi}, \mathbf{x})$, $\mathbf{W}(\boldsymbol{\xi}, \mathbf{x})$ and $\mathbf{F}(\boldsymbol{\xi})$ depend upon coordinates, the weight function, and values of the function f(**x**) at all particles in the compact support of $W(\boldsymbol{\xi}, \mathbf{x})$. Eq. (2.5) can be written as

$$\mathbf{C}(\boldsymbol{\xi}, \mathbf{x})\, \mathbf{Q}(\mathbf{x}) = \mathbf{D}(\boldsymbol{\xi}, \mathbf{x})\, \mathbf{F}(\boldsymbol{\xi}), \tag{2.6}$$

where $\mathbf{C}(\boldsymbol{\xi}, \mathbf{x}) = \mathbf{H}(\boldsymbol{\xi}, \mathbf{x})\, \mathbf{W}(\boldsymbol{\xi}, \mathbf{x})\, \mathbf{H}^{\mathrm{T}}(\boldsymbol{\xi}, \mathbf{x})$, $\mathbf{D}(\boldsymbol{\xi}, \mathbf{x}) = \mathbf{H}(\boldsymbol{\xi}, \mathbf{x})\, \mathbf{W}(\boldsymbol{\xi}, \mathbf{x})$.

Thus, $\mathbf{Q}(\mathbf{x})$ can be found from Eq. (2.6) by inverting $\mathbf{C}(\boldsymbol{\xi}, \mathbf{x})$. That is,

$$\mathbf{Q}(\mathbf{x}) = \left[\mathbf{C}(\boldsymbol{\xi}, \mathbf{x})\right]^{-1} \mathbf{D}(\boldsymbol{\xi}, \mathbf{x})\, \mathbf{F}(\boldsymbol{\xi}) = \mathbf{K}(\boldsymbol{\xi}, \mathbf{x})\, \mathbf{F}(\boldsymbol{\xi}), \tag{2.7}$$

where $\mathbf{K}(\boldsymbol{\xi}, \mathbf{x}) = \left[\mathbf{C}(\boldsymbol{\xi}, \mathbf{x})\right]^{-1} \mathbf{D}(\boldsymbol{\xi}, \mathbf{x})$. The sufficient condition for the matrix $\mathbf{C}(\boldsymbol{\xi}, \mathbf{x})$ to be invertible is that the number, N(**x**), of particles in the compact support of $\mathbf{W}(\boldsymbol{\xi}, \mathbf{x})$ equals at least the number of unknowns in matrix **Q**(**x**) [8]. The first two rows and the fifth row of elements of the matrix Q(**x**) can be explicitly written as

$$f(\mathbf{x}) = \sum_{i=1}^{N(\mathbf{x})} K_{1i} F_i, \tag{2.8}$$

$$\frac{\partial f(\mathbf{x})}{\partial x_1} = \sum_{i=1}^{N(\mathbf{x})} K_{2i} F_i, \tag{2.9}$$

$$\frac{1}{2}\frac{\partial^2}{\partial x_1^2} f(\mathbf{x}) = \sum_{i=1}^{N(\mathbf{x})} K_{5i} F_i. \tag{2.10}$$

In the FE terminology, functions K_{1i}, K_{2i} and $2K_{5i}$ are shape functions for $f(\mathbf{x})$, $\partial f(\mathbf{x})/\partial x_1$ and $\partial^2 f(\mathbf{x})/\partial x_1^2$, respectively. We note that $K_{2i} \neq \partial K_{1i}/\partial x_1$ and $2K_{5i} \neq \partial K_{2i}/\partial x_1$.

2.2 Moving least squares basis (MLS) functions

Consider a function $f(\mathbf{x})$ of variable **x** defined in the domain Ω. The function $f(\mathbf{x})$ can be approximated by the function $f^{h}(\mathbf{x})$ defined by

$$f^{h}(\mathbf{x}) = \mathbf{P}^{\mathrm{T}}(\mathbf{x})\, \mathbf{a}(\mathbf{x}), \tag{2.11}$$

where $\mathbf{P}^{\mathrm{T}}(\mathbf{x})$ is a complete polynomial of order m and $\mathbf{a}(\mathbf{x})$ is a vector of undefined coefficients. Examples of $\mathbf{P}^{\mathrm{T}}(\mathbf{x})$ for a two-dimensional (2-D) problem with **x** = (x, y) are:

$\mathbf{P}^{\mathrm{T}}(\mathbf{x}) = [1, x, y]$, n = 3,
first order complete polynomial,

$\mathbf{P}^{\mathrm{T}}(\mathbf{x}) = \left[1, x, y, x^2, xy, y^2\right]$, n = 6,
second order complete polynomial.

We define the weighted discrete L^2 norm J by

$$J(\mathbf{a}(\mathbf{x})) = \sum_{I=1}^{N(\mathbf{x})} W^{I}(\mathbf{x})(\mathbf{P}^{\mathrm{T}}\left(\mathbf{x}^{I}\right)\mathbf{a}(\mathbf{x}) - \hat{u}_I)^2, \tag{2.12}$$

where $W^{I}(\mathbf{x}) = W\left(\mathbf{x} - \mathbf{x}^{I}\right)$ is the weight function of compact support associated with particle I having coordinates $\mathbf{x}^{I}$, $\hat{u}_I$ is the fictitious value of the function $f(\mathbf{x})$ at the point $\mathbf{x}^{I}$ and N(**x**) is the number of particles in the compact support of $W^{I}(\mathbf{x})$. Values of coefficients $\mathbf{a}(\mathbf{x})$ are determined by minimizing $J(\mathbf{a}(\mathbf{x}))$ with respect to $\mathbf{a}(\mathbf{x})$. That is,

$$\frac{\partial J(\mathbf{a}(\mathbf{x}))}{\partial \mathbf{a}} = \mathbf{0} \Rightarrow \mathbf{A}(\mathbf{x})\, \mathbf{a}(\mathbf{x}) = \mathbf{B}(\mathbf{x})\, \hat{\mathbf{u}}, \tag{2.13}$$

where

$$\mathbf{A}(\mathbf{x}) = \sum_{I=1}^{N(\mathbf{x})} W^{I}(\mathbf{x}) \mathbf{P}\left(\mathbf{x}^{I}\right) \mathbf{P}^{\mathrm{T}}\left(\mathbf{x}^{I}\right),$$

$$\mathbf{B}(\mathbf{x}) = \left[W^{1}(\mathbf{x})\, \mathbf{P}\left(\mathbf{x}^{1}\right), W^{2}(\mathbf{x})\, \mathbf{P}\left(\mathbf{x}^{2}\right), \ldots, W^{\mathrm{N(x)}}(\mathbf{x})\, \mathbf{P}\left(\mathbf{x}^{\mathrm{N(x)}}\right)\right],$$

$$\hat{\mathbf{u}}^{\mathbf{T}} = \left[\hat{u}_1, \hat{u}_2, \ldots, \hat{u}_{\mathrm{N(x)}}\right].$$

Eq. (2.13) gives

$$\mathbf{a}(\mathbf{x}) = \mathbf{A}^{-1}(\mathbf{x})\, \mathbf{B}(\mathbf{x})\, \hat{\mathbf{u}}. \tag{2.14}$$

Journal: 466 MS: 0700 TYPESET DISK LE CP Disp.:2012/3/24 Pages: 16 Layout: Large

Substituting for $\mathbf{a}(\mathbf{x})$ from Eq. (2.14) into Eq. (2.11) we get

$$f^h(\mathbf{x}) = \sum_{I=1}^{N(\mathbf{x})} \phi^I(\mathbf{x})\hat{u}_I, \tag{2.15}$$

where

$$\phi^I(\mathbf{x}) = \sum_{J=1}^{n} P_J(\mathbf{x})\,[\mathbf{A}^{-1}(\mathbf{x})\,\mathbf{B}(\mathbf{x})]_{JI},$$

and $\phi^I(\mathbf{x})$ is the MLS basis function. Unlike the SSPH basis functions, in which derivatives of function $f(\mathbf{x})$ are expressed in terms of basis functions that are different from those used to approximate $f(\mathbf{x})$, in the MLS basis functions the approximation of derivatives of $f(\mathbf{x})$ requires that the MLS basis functions be differentiable. The spatial derivatives of basis function $\phi^I(\mathbf{x})$ are given by

$$\phi^I_{,k}(\mathbf{x}) = \sum_{J=1}^{n} \Big\{ P_{J,k}[\mathbf{A}^{-1}(\mathbf{x})\,\mathbf{B}(\mathbf{x})]_{JI} + P_J[\mathbf{A}^{-1}(\mathbf{x})\,\mathbf{B}_{,k}(\mathbf{x}) + (\mathbf{A}^{-1}(\mathbf{x}))_{,k}\mathbf{B}(\mathbf{x})]_{JI} \Big\}, \tag{2.16}$$

where $\phi^I_{,k}(\mathbf{x}) = \partial\phi^I(\mathbf{x})/\partial x_k$.

2.3 Meshless approximations with consistent pseudo-derivatives

The approximation $u^h(\mathbf{x})$ of the function $u(\mathbf{x})$ is defined by

$$u^h(\mathbf{x}) = \sum_{I=1}^{N(\mathbf{x})} \phi^I(\mathbf{x})u_I, \tag{2.17}$$

where $\phi^I(\mathbf{x})$ are basis functions, $N(\mathbf{x})$ is the number of basis functions, and u_I are the particle parameters associated with particle I having coordinates $\mathbf{x}$. In order that basis functions exactly reproduce a polynomial of degree 1, we must have

$$\sum_{I=1}^{N(\mathbf{x})} \phi^I(\mathbf{x}) = 1, \quad \sum_{I=1}^{N(\mathbf{x})} \phi^I(\mathbf{x})x_I = x, \quad \sum_{I=1}^{N(\mathbf{x})} \phi^I(\mathbf{x})y_I = y, \tag{2.18}$$

Differentiation of both sides of Eq. (2.18) with respect to x and y gives

$$\sum_{I=1}^{N(\mathbf{x})} \phi^I_{,x}(\mathbf{x}) = 0, \quad \sum_{I=1}^{N(\mathbf{x})} \phi^I_{,y}(\mathbf{x}) = 0, \tag{2.19a}$$

$$\sum_{I=1}^{N(\mathbf{x})} \phi^I_{,x}(\mathbf{x})x_I = 1, \quad \sum_{I=1}^{N(\mathbf{x})} \phi^I_{,y}(\mathbf{x})x_I = 0, \tag{2.19b}$$

$$\sum_{I=1}^{N(\mathbf{x})} \phi^I_{,x}(\mathbf{x})y_I = 0, \quad \sum_{I=1}^{N(\mathbf{x})} \phi^I_{,y}(\mathbf{x})y_I = 1, \tag{2.19c}$$

where a comma followed by x denotes the derivative with respect to x.

In the pseudo-derivatives method [10], the derivatives of $u^h(\mathbf{x})$ are approximated by using basis functions that are not necessarily derivatives of $\phi^I(\mathbf{x})$. Thus,

$$u^h_{,x}(\mathbf{x}) = \sum_{I=1}^{N(\mathbf{x})} G^I_x(\mathbf{x})u_I \tag{2.20a}$$

$$u^h_{,y}(\mathbf{x}) = \sum_{I=1}^{N(\mathbf{x})} G^I_y(\mathbf{x})u_I, \tag{2.20b}$$

where $G^I_x(\mathbf{x})$ and $G^I_y(\mathbf{x})$ are basis functions for the derivatives. Krongauz and Belytschko [10] assume that $G^I_x(\mathbf{x})$ and $G^I_y(\mathbf{x})$ are the linear combination of the first-order derivatives of the Shepard approximation functions ϕ^I_0. That is,

$$G^I_x(\mathbf{x}) = \alpha_1(\mathbf{x})\,\phi^I_{0,x} + \alpha_2(\mathbf{x})\,\phi^I_{0,y}, \tag{2.21a}$$

$$G^I_y(\mathbf{x}) = \beta_1(\mathbf{x})\,\phi^I_{0,x} + \beta_2(\mathbf{x})\,\phi^I_{0,y}, \tag{2.21b}$$

where α_I and β_I (I = 1,2) are unknown functions to be determined as outlined below. Note that the Shepard approximation functions have the property of partition of unity so that Eqs. (2.19a) are automatically satisfied. Substitution from Eqs. (2.21) into Eqs. (2.19b) and (2.19c) gives

$$\mathbf{A}(\mathbf{x})\mathbf{B} = \mathbf{r}, \tag{2.22}$$

where

$$\mathbf{A}(\mathbf{x}) = \begin{bmatrix} \mathbf{a}(\mathbf{x}) & 0 \\ 0 & \mathbf{a}(\mathbf{x}) \end{bmatrix},$$

$$\mathbf{a}(\mathbf{x}) = \sum_{I=1}^{N(\mathbf{x})} \begin{bmatrix} \phi^I_{0,x}x_I & \phi^I_{0,y}x_I \\ \phi^I_{0,x}y_I & \phi^I_{0,y}y_I \end{bmatrix},$$

$$\mathbf{B} = \begin{Bmatrix} \alpha_1 \\ \alpha_2 \\ \beta_1 \\ \beta_2 \end{Bmatrix}, \mathbf{r} = \begin{Bmatrix} 1 \\ 0 \\ 0 \\ 1 \end{Bmatrix}.$$

Thus α_I and β_I (I = 1,2) can be found by solving Eq. (2.22).

3 Weak formulation of two-dimensional elastostatics problems

With respect to rectangular Cartesian coordinates, the balance of linear momentum for static 2-D deformations of a body occupying the domain Ω is

$$\sigma_{ij,j} + b_i = 0, \text{ in } \Omega, i = 1, 2, \tag{3.1}$$

where σ_{ij} is the Cauchy stress and b_i is the body force per unit volume. Henceforth we neglect the body force. For simplicity, we write boundary conditions as

$$u_i = \bar{u}_i, \text{ on } \Gamma_u, \tag{3.2}$$

$$\sigma_{ij}n_j = \bar{t}_i, \text{ on } \Gamma_t. \tag{3.3}$$

Eq. (3.2) is essential boundary condition, $\bar{\mathbf{u}}$ is prescribed displacement on boundary Γ_u, Eq. (3.3) is natural boundary condition, $\bar{\mathbf{t}}$ is prescribed traction on boundary Γ_t, and $\mathbf{n}$ is a unit outward normal to boundary Γ_t. The constitutive equation for 2-D deformations of a linear elastic homogeneous and isotropic material can be written as

$$\boldsymbol{\sigma} = \mathbf{D}\boldsymbol{\varepsilon}, \tag{3.4}$$

where $\mathbf{D}$ is a matrix of elastic constants and $\boldsymbol{\varepsilon}$ is the strain tensor corresponding to infinitesimal deformations. The 3 × 3 matrix $\mathbf{D}$ and the 3 x 1 matrix $\boldsymbol{\varepsilon}$ can be written as

$$\mathbf{D} = \frac{E'}{1-(\upsilon')^2}\begin{bmatrix} 1 & \upsilon' & 0 \\ \upsilon' & 1 & 0 \\ 0 & 0 & \frac{1-\upsilon'}{2} \end{bmatrix}, \tag{3.5}$$

$$\boldsymbol{\varepsilon} = \begin{bmatrix} \varepsilon_{11} \\ \varepsilon_{22} \\ 2\varepsilon_{12} \end{bmatrix}, \tag{3.6}$$

where $E' = \frac{E}{1-\upsilon^2}$, $\upsilon\prime = \frac{\upsilon}{1-\upsilon}$ for plane strain, and $E' = E$, $\upsilon\prime = \upsilon$ for plane stress deformations, E is Young's modulus, and υ is Poisson's ratio.

The strain-displacement relation can be expressed as

$$\boldsymbol{\varepsilon} = \mathbf{L}\mathbf{u}, \tag{3.7}$$

where the displacement vector $\mathbf{u}$ and the matrix operator $\mathbf{L}$ are given by

$$\mathbf{u} = \begin{bmatrix} u_1 \\ u_2 \end{bmatrix}, \mathbf{L} = \begin{bmatrix} \frac{\partial}{\partial X_1} & 0 \\ 0 & \frac{\partial}{\partial X_2} \\ \frac{\partial}{\partial X_2} & \frac{\partial}{\partial X_1} \end{bmatrix}. \tag{3.8}$$

Substitution into Eq. (3.1) for stresses from Eq. (3.4) and for strains from Eq. (3.7) gives two coupled partial differential equations for displacements u_1 and u_2 which are to be solved under boundary conditions (3.2) and (3.3).

The meshless local Petrov-Galerkin (MLPG) formulation is used to find an approximate solution of the above mentioned BVP. Consider a finite number of particles distributed in the domain Ω. For the particle I with coordinates x_i^i, we derive a local weak form of Eq. (3.1) by taking the inner product of both sides of Eq. (3.1) with a weight function W_i^I of compact support Ω_q with the boundary Γ_q and integrating the resulting equation. The result is

$$\int_{\Omega_q} W_i^I \sigma_{ij,j} d\Omega = 0. \tag{3.9}$$

Essential boundary condition (3.2) is satisfied by using the penalty method. We take the inner product of Eq. (3.2) with W_i^I, integrate the resulting equation on Γ_q^u, multiply with the penalty parameter α, and combine it with Eq. (3.9) to arrive at

$$\int_{\Omega_q} W_i^I \sigma_{ij,j} d\Omega - \alpha \int_{\Gamma_q^u} W_i^I (u_i - \bar{u}_i)\, d\Gamma = 0. \tag{3.10}$$

Here $\Gamma_q^u = \Gamma_q \cap \Gamma_u$. In Eq. (3.10) we have taken, for simplicity, α to be the same for every particle on Γ_q^u. However, it could have been taken to be function of $\mathbf{x}$. We integrate the first term on the left-hand side of Eq. (3.10) by parts, use the divergence theorem, and boundary condition (3.3) to obtain

$$\int_{\Omega_q} W_i^I \sigma_{ij,j} d\Omega = \int_{\Gamma_q} W_i^I \sigma_{ij,n_j} d\Gamma - \int_{\Omega_q} W_{i,j}^I \sigma_{ij,j} d\Omega. \tag{3.11}$$

Substituting from Eq. (3.11) into Eq. (3.10), the following weak form is obtained

$$\int_{\Gamma_q} W_i^I \sigma_{ij} n_j d\Gamma - \int_{\Omega_q} W_{i,j}^I \sigma_{ij} d\Omega - \alpha \int_{\Gamma_q^u} W_i^I (u_i - \bar{u}_i)\, d\Gamma = 0. \tag{3.12}$$

Let $\Gamma_q = \Gamma_q^u \cup \Gamma_q^t \cup \Gamma_q^I$, $\Gamma_q^t = \Gamma_q \cap \Gamma_t$, $\Gamma_q^I = \Gamma_q - \Gamma_q^u - \Gamma_q^t$. Recalling that weight function W_i^I vanishes on boundary Γ_q^I, Eq. (3.12) can be simplified to

$$\int_{\Omega_q} W_{i,j}^I \sigma_{ij} d\Omega + \alpha \int_{\Gamma_q^u} W_i^I u_i d\Gamma - \int_{\Gamma_q^u} W_i^I \sigma_{ij} n_j d\Gamma = \int_{\Gamma_q^t} W_i^I \bar{t}_i d\Gamma + \alpha \int_{\Gamma_q^u} W_i^I \bar{u}_i d\Gamma. \tag{3.13}$$

Eq. (3.13) in the matrix form can be written as

$$\int_{\Omega_q} (\mathbf{LW})^T \mathbf{D}\mathbf{L}\mathbf{u} d\Omega + \alpha \int_{\Gamma_q^u} \mathbf{W}\mathbf{u} d\Gamma - \int_{\Gamma_q^u} \mathbf{W}\mathbf{N}\mathbf{D}\mathbf{L}\mathbf{u}\, d\Gamma = \int_{\Gamma_q^t} \mathbf{W}\bar{\mathbf{t}} d\boldsymbol{\Gamma} + \alpha \int_{\Gamma_q^u} \mathbf{W}\bar{\mathbf{u}} d\boldsymbol{\Gamma}, \tag{3.14}$$

where matrices $\mathbf{W}$ and $\mathbf{N}$ are given by

$$\mathbf{N} = \begin{bmatrix} n_1 & 0 & n_2 \\ 0 & n_2 & n_1 \end{bmatrix}, \mathbf{W} = \begin{bmatrix} W^I & 0 \\ 0 & W^I \end{bmatrix}.$$

Eq. (3.14) is the local weak form of the BVP defined by Eqs. (3.1) through (3.8).

Let ϕ^I be either the SSPH or the MLS basis function associated with particle $\mathbf{x}^I$. Then trial solutions for displacements u_1 and u_2 can be expressed as

$$\mathbf{u}^I = \begin{bmatrix} u_1^I \\ u_2^I \end{bmatrix} = \phi^I \hat{u} = \begin{bmatrix} \phi_1^I & 0 & \cdots & \phi_N^I & 0 \\ 0 & \phi_1^I & \ldots & 0 & \phi_N^I \end{bmatrix} \begin{bmatrix} \hat{u}_1^1 \\ \hat{u}_2^1 \\ \vdots \\ \hat{u}_1^N \\ \hat{u}_2^N \end{bmatrix}, \tag{3.15}$$

where N = N($\mathbf{x}$) is the number of particles in the compact support of W^I. For the SSPH basis functions, we substitute

Journal: 466 MS: 0700 TYPESET DISK LE CP Disp.:2012/3/24 Pages: 16 Layout: Large

for ϕ^I from Eq. (2.8) and get

$$\mathbf{u}^I = \begin{bmatrix} K^I_{11} & 0 & \cdots K^I_{1N} & 0 \\ 0 & K^I_{11} & \cdots 0 & K^I_{1N} \end{bmatrix} \begin{bmatrix} \hat{u}^1_1 \\ \hat{u}^1_2 \\ \vdots \\ \hat{u}^N_1 \\ \hat{u}^N_2 \end{bmatrix}$$

$$= \sum_{J=1}^{N} \left\{ \begin{bmatrix} K^I_{1J} & 0 \\ 0 & K^I_{1J} \end{bmatrix} \begin{bmatrix} \hat{u}^J_1 \\ \hat{u}^J_2 \end{bmatrix} \right\}. \tag{3.16}$$

Since the SSPH basis function for spatial derivatives of a function are different from those for the function, we have

$$\mathbf{L}\mathbf{u}^I = \sum_{J=1}^{N} \left\{ \begin{bmatrix} K^I_{2J} & 0 \\ 0 & K^I_{3J} \\ K^I_{3J} & K^I_{2J} \end{bmatrix} \begin{bmatrix} \hat{u}^J_1 \\ \hat{u}^J_2 \end{bmatrix} \right\}. \tag{3.17}$$

Substitution from Eqs. (3.16) and (3.17) into Eq. (3.14) gives

$$\sum_{J=1}^{N} \mathbf{K}'_{IJ} \hat{\mathbf{u}}^J = \mathbf{F}_I, \tag{3.18}$$

where

$$\mathbf{K}'_{IJ} = \int_{\Omega_q} (\mathbf{L}\mathbf{W}^I)^T \mathbf{D}\mathbf{V}_J d\Omega + \alpha \int_{\Gamma^u_q} \mathbf{W}^I \mathbf{M}_J d\Gamma - \int_{\Gamma^u_q} \mathbf{W}^I \mathbf{N}\mathbf{D}\mathbf{V}_J d\Gamma,$$

$$\mathbf{F}_I = \int_{\Gamma^t_q} \mathbf{W}^I \bar{\mathbf{t}}\, d\Gamma + \alpha \int_{\Gamma^u_q} \mathbf{W}^I \bar{\mathbf{u}}\, d\Gamma,$$

$$\mathbf{V}_J = \begin{bmatrix} K^I_{2J} & 0 \\ 0 & K^I_{3J} \\ K^I_{3J} & K^I_{2J} \end{bmatrix}, \mathbf{M}_J = \begin{bmatrix} K^I_{1J} & 0 \\ 0 & K^I_{1J} \end{bmatrix}.$$

We derive an algebraic equation similar to Eq. (3.18) for each particle in the domain Ω, thereby obtain the number of equations equal to the number of unknowns. There is no assembly of equations required in a meshless method.

For the MLS basis functions the local weak form of the BVP defined by Eqs. (3.1) through (3.8) has been derived, amongst others, by Ching and Batra [14] and the derivation is omitted here.

4 Numerical results for example problems

4.1 Plane stress deformations of a cantilever beam

Consider plane stress deformations of a cantilever like beam of length L = 8.0 mm, H = 1.0 mm, and width = 1.0 mm, as shown in Fig. 2. The beam material is assumed to be linear elastic and isotropic having E = 1GPa, $\upsilon = 0.25$. The analytical solution [15] for displacements and stresses is

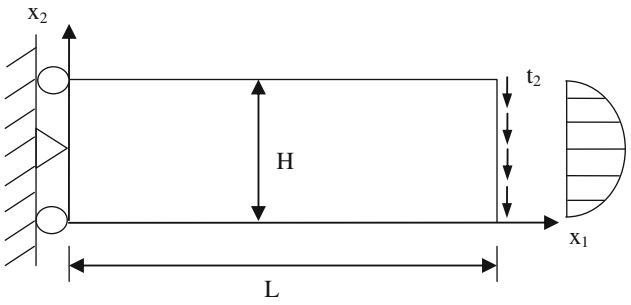

Fig. 2 A cantilever like beam subjected to tangential tractions at the right edge

$$u_1 = -\frac{F}{6EI}(x_2 - \frac{H}{2})\,[3x_1\,(2L - x_1) + (2+\upsilon)\,x_2\,(x_2 - H)]\,,$$

$$u_2 = \frac{F}{6EI}\left[x_1^2\,(3L - x_1) + 3\upsilon(L - x_1)(x_2 - \frac{H}{2})^2 + \frac{4+5\upsilon}{4}H^2 x_1\right], \tag{4.1}$$

$$I = \frac{H^3}{12},$$

$$\sigma_{11} = -\frac{F}{I}(L - x_1)\left(x_2 - \frac{H}{2}\right),$$

$$\sigma_{22} = 0, \tag{4.2}$$

$$\sigma_{12} = -\frac{Fx_2}{2I}(x_2 - H)\,,$$

where F is resultant of tangential tractions applied at the unclamped end and I is the second moment of area of cross-section of the beam about the x_3-axis passing through the centroid of the cross-section. Displacements (4.1) at particles on the left edge are applied. Surface tractions are given by

$$t_1 = 0, t_2 = 0, \text{ on the bottom and the top surfaces,}$$

$$t_1 = 0, t_2 = -\frac{Fx_2}{2I}(x_2 - H)\,, \text{ on the right surface.}$$

Results have been computed for F = 1N and the penalty parameter α in Eq. (3.10) is set equal to 10^9.

We compare results computed by using the SSPH and the MLS basis functions, and ascertain the effect on the computed results of the weight function, the number N of particles, the order m of the complete polynomials in the basis functions, and the size of the compact support as determined by the smoothing length h and the compact support parameter β. The smoothing length, h, equals the distance between the particle of interest and its nearest neighboring particle, and β is the scaling factor for determining the domain of influence for the weight function.

4.1.1 Effect of the weight function W_I

A set of 21 × 5 particles with 21 uniformly spaced particles along the x_1-direction and 5 uniformly spaced particles along the x_2-direction is used. The integrals on Ω appearing in Eq. (3.14) are evaluated by using the 9 x 9 Gauss integration rule and those on Γ by employing the 9 Gauss point integration rule. The compact support domain factor $\beta$is taken to be 4.0. Second order ($m = 2$) complete polynomials are employed to generate the MLS basis functions and the first three terms are kept in the Taylor series (2.1). Three different weight functions, namely, the cubic spline [16], the quartic spline [17], and the Gaussian function [18] are used to generate the SSPH and the MLS basis functions.

Cubic spline function:

$$W_I(d) = \frac{2}{3}\begin{cases} 1 - 6d^2 + 6d^3, & 0 \le d \le 0.5, \\ 2 - 6d + 6d^2 - 2d^3, & 0.5 \le d \le 1, \\ 0, & 1 < d. \end{cases} \tag{4.3}$$

Quartic spline function:

$$W_I(d) = \frac{5}{8}\begin{cases} 1 - 6d^2 + d^3 - 3d^4, & 0 \le d \le 1, \\ 0, & 1 < d. \end{cases} \tag{4.4}$$

Gaussian function:

$$W_I(d) = \frac{1}{1 - e^{-4}}\begin{cases} e^{-4d} - e^{-4}, & 0 \le d \le 1, \\ 0, & 1 < d, \end{cases} \tag{4.5}$$

where $d = \left|\boldsymbol{\xi} - \mathbf{x}^I\right| / \beta h$.

In Fig. 3 we have compared, for the three weight functions, the variation of the displacement u_2 along the top edge of the beam by using the SSPH and the MLS basis functions.

It is evident from these plots that in each case the computed results agree well with the analytical solution of the problem. In order to quantify the difference between the analytical and the numerical solutions, we define the error norm, E_0^u and E_0^σ, in terms of the displacement and the stress field, respectively.

$$E_0^u = \sqrt{\frac{\sum_{i=1}^{M}(u^i_{numerical} - u^i_{analytical})^2}{\sum_{i=1}^{M}(u^i_{analytical})^2}},$$

$$E_0^\sigma = \sqrt{\frac{\sum_{i=1}^{M}(\sigma^i_{numerical} - \sigma^i_{analytical})^2}{\sum_{i=1}^{M}(\sigma^i_{analytical})^2}}. \tag{4.6}$$

where M is the number of particles in the entire domain.

From values of E_0^u and E_0^σ for the six sets of results listed in Table 1, we conclude that the Gaussian weight function gives the least value of E_0^u for the u_2 displacement and E_0^σ for the σ_{11} stress. We note that both the cubic and the quartic spline weight functions also give reasonably accurate values of the u_2-displacement, and the σ_{11} stress. For each weight function the MLS basis functions give a smaller value of E_0^u and E_0^σ than that given by the SSPH basis functions.

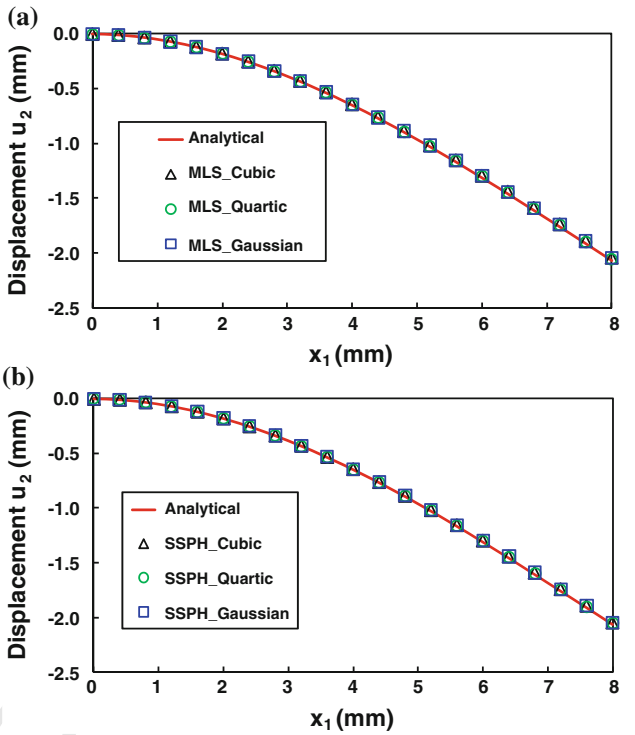

Fig. 3 For the three weight functions, namely, the cubic spline, the quartic spline and the Gaussian, comparison with the analytical solution of the displacement u_2 along the top surface computed by using **a** the MLS, and **b** the SSPH basis functions

Table 1 The error norm (a) E_0^u and (b)E_0^σ in the u_2-displacement and the σ_{11} stress for the three weight functions

Basis function	W^I		
	Cubic	Quartic	Gaussian
(a)			
MLS	0.0204	0.0190	0.0182
SSPH	0.0322	0.0410	0.0306
(b)			
MLS	0.0295	0.0165	0.0141
SSPH	0.0248	0.0295	0.0166

4.1.2 Effect of the number of particles

For the Gaussian weight function (4.5), we have listed in Table 2 values of E_0^u and E_0^σ for particles placed in uniform rectangular grids of 21 × 5, 33 × 5, and 33 × 9 particles. As expected the error norm decreases monotonically with an increase in the number of particles along the x_1- and the x_2- directions. For each distribution of particles, the error norms have smaller values for the MLS basis functions as compared to those for the SSPH basis functions. In the following analysis, 33 × 9 particles are used to find an approximate solution of the problem.

Journal: 466 MS: 0700 TYPESET DISK LE CP Disp.:2012/3/24 Pages: 16 Layout: Large

Table 2 For the two basis functions, the error norm (a) E_0^u and (b) E_0^σ in the u_2-displacement and the σ_{11} stress for three distributions of particles

Basis function	$N_1 \times N_2$		
	21×5	33×5	33×9
(a)			
MLS	0.0182	0.0157	0.0108
SSPH	0.0306	0.0278	0.0242
(b)			
MLS	0.0141	0.0119	0.0106
SSPH	0.0166	0.0145	0.0129

Table 3 For the two basis functions, the CPU time (in seconds) for different values of β

Basis function	β						
	3.0	3.5	4.0	4.5	5.0	6.0	8.0
MLS	24.89	29.88	33.92	38.13	41.05	47.53	59.94
SSPH	23.67	26.09	28.16	30.30	32.42	36.28	43.30

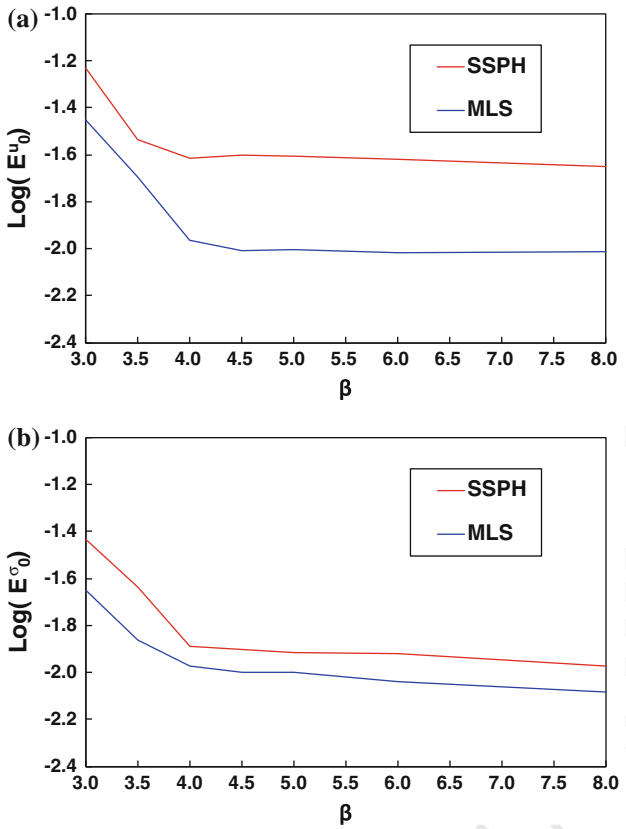

Fig. 4 Variation of the **a** $\log(E_0^u)$, and **b** $\log(E_0^\sigma)$ for the u_2-displacement and the σ_{11} stress with the compact support domain parameter β

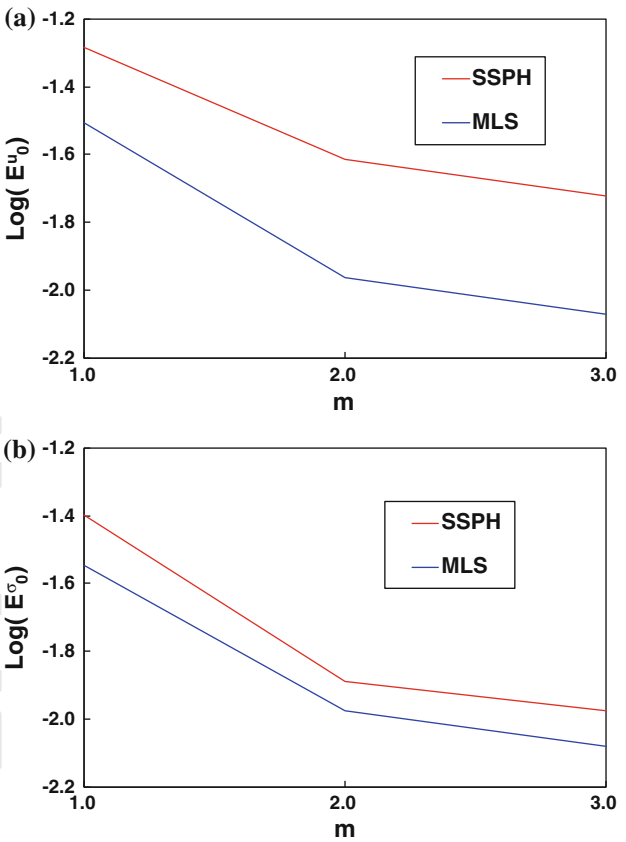

Fig. 5 Variation of the **a** $\log(E_0^u)$, and **b** $\log(E_0^\sigma)$ for the u_2-displacement and the σ_{11} stress with the order, m, of the complete polynomials used to generate basis functions

4.1.3 Effect of the size of the compact support

For second order ($m = 2$) complete polynomials used to generate the SSPH and the MLS basis functions, the support domain parameter β should be large enough for Ω^I to include at least six particles to ensure that matrix $\mathbf{C}(\boldsymbol{\xi}, \mathbf{x})$ is non-singular. In Fig. 4 we have plotted $\log(E_0^u)$ for the u_2 displacement and $\log(E_0^\sigma)$ for the σ_{11} stress vs. β for the two basis functions. It is clear that in each case the error norm decreases rather rapidly when β is increased from 3.0 to 4.0. However, for $\beta > 4$ the error norm remains essentially unchanged. The CPU times for different values of β are listed in Table 3. We note that the computational cost noticeably increases with an increase in the value of β, and is higher by 5% for $\beta = 3$ and 38% for $\beta = 8$ for the MLS basis functions than that for the SSPH basis functions. Results presented below are computed by taking $\beta = 4.0$.

4.1.4 Effect of the order of the complete polynomials in the basis functions

We note that for $\beta = 4$, one can consider up to third order complete polynomials (i.e., m = 3) in the basis functions and still satisfy the invertibility of matrix $\mathbf{C}(\boldsymbol{\xi}, \mathbf{x})$ appearing in Eq. (2.7). Values of $\log(E_0^u)$ and $\log(E_0^\sigma)$ for m = 1, 2 and

Journal: 466 MS: 0700 TYPESET DISK LE CP Disp.:2012/3/24 Pages: 16 Layout: Large

Table 4 For the two basis functions, the CPU time (in seconds) for different values of m

Basis function	m		
	1	2	3
MLS	12.72	33.92	88.63
SSPH	10.48	28.16	71.55

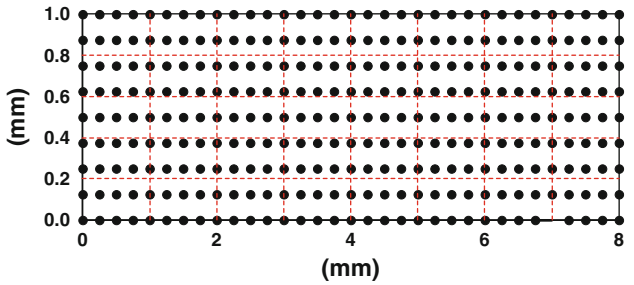

Fig. 6 Background mesh (40 elements with 297 particles) for the cantilever beam problem used only to evaluate the domain integral in Eq. (4.7)

3 plotted in Fig. 5 reveal the expected result that the error decreases with an increase in the value of m. The CPU time for different values of m is listed in Table 4. Of course, the computational cost increases with an increase in the value of m, and is about 20% higher for the MLS basis functions than that for the SSPH basis functions. Henceforth, we set $m = 2$ as a compromise between the computational cost and the error in the computed solution.

4.1.5 Convergence rate

To find the rate of convergence of numerical solutions with respect to the distance between adjacent particles, we use the strain energy error norm defined as

$$\mathrm{E_e} = \sqrt{\int_\Omega \frac{1}{2}\left(\boldsymbol{\varepsilon}_{\text{numerical}} - \boldsymbol{\varepsilon}_{\text{analytical}}\right) : \left(\boldsymbol{\sigma}_{\text{numerical}} - \boldsymbol{\sigma}_{\text{analytical}}\right) \mathrm{d}\Omega}, \tag{4.7}$$

where $\boldsymbol{\varepsilon}$ and $\boldsymbol{\sigma}$ are strain and stress tensors, respectively, and ":" implies the inner product between two 2nd order tensors. The integral is evaluated by using the background mesh depicted in Fig. 6.

The problem is also analyzed using the pseudo-derivative (PD) basis functions (2.21). The plot of strain energy error norm versus the minimum distance h between two adjacent particles for the three basis functions is shown in Fig. 7. We note that the convergence rate equals 1.43, 1.44 and 1.47, respectively, for the PD, the SSPH and the MLS basis functions.

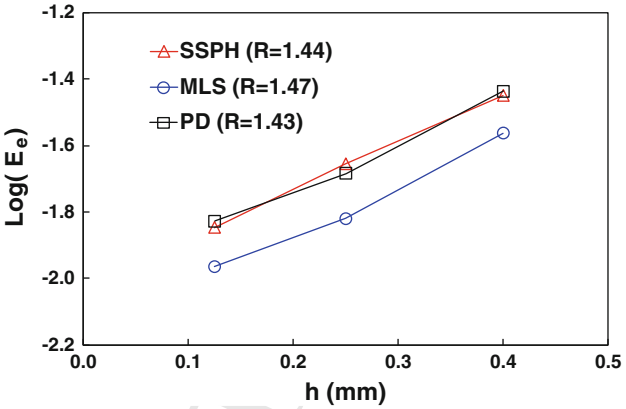

Fig. 7 Convergence of strain energy error norm for the SSPH, MLS and PD basis functions

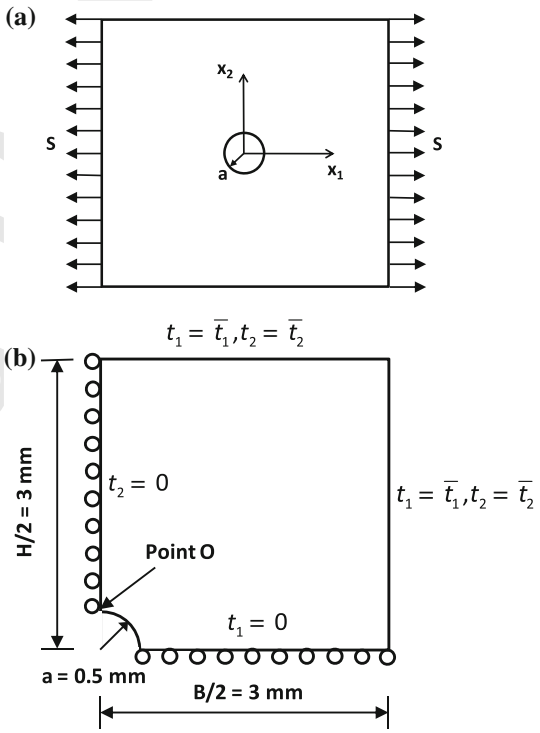

Fig. 8 **a** An infinite plate with a hole at the center subjected to surface tractions in the x_1-direction at the edges, and **b** boundary conditions applied at edges of a quarter of the plate

4.2 Stress concentration in an infinite square plate with a circular hole at the centroid and subjected to uniform tensile tractions at opposite edges

Consider an infinite square plate, shown in Fig. 8a, made of a linear elastic, homogeneous and isotropic material with a circular hole of radius a at the plate centroid and subjected to uniform axial tensile tractions of magnitude S at opposite edges that are at infinity. The analytical

Journal: 466 MS: 0700 TYPESET DISK LE CP Disp.:2012/3/24 Pages: 16 Layout: Large

solution [15] for the stress fields in cylindrical coordinates (r, θ) with the origin located at the hole center and based on the assumption of a plane strain state of deformation is

$$\sigma_{rr} = \frac{S}{2}\left(1 - \frac{a^2}{r^2}\right) + \frac{S}{2}\left(1 + \frac{3a^4}{r^4} - \frac{4a^2}{r^2}\right)\cos 2\theta,$$
$$\sigma_{\theta\theta} = \frac{S}{2}\left(1 + \frac{a^2}{r^2}\right) - \frac{S}{2}\left(1 + \frac{3a^4}{r^4}\right)\cos 2\theta, \qquad (4.8)$$
$$\sigma_{r\theta} = -\frac{S}{2}\left(1 - \frac{3a^4}{r^4} + \frac{2a^2}{r^2}\right)\sin 2\theta.$$

Due to symmetry of the problem about the horizontal and the vertical centroidal axes, deformations of only a quarter of the finite plate are analyzed. Boundary conditions arising from symmetry of the problem are applied to the left vertical and the bottom horizontal edges and the hole surface is traction free. Since we analyze a finite size specimen, the normal and tangential surface tractions in rectangular Cartesian coordinates applied on the edges in Fig. 8b are found from Eq. (4.8) by using tensor transformation rules, and the BVP is numerically solved with the SSPH, MLS and PD methods for E = 1MPa, $\upsilon = 0.25$, and S = 1MPa. Parameters for generating the SSPH and the MLS basis functions are: $m = 2$, Gaussian weight function, $\beta = 4.0$, h = distance between the particle of interest and its nearest neighbor, 9×9 Gauss integration rule for area integration, and 9 Gauss points for line integration. Fig. 9 depicts the distribution of 135, 297 and 369 particles with 18, 15 and 9 particles on the quarter circle, respectively. Variations of the displacement u_2 and of the stress σ_{11} along the x_2-direction are exhibited in Figs. 10 and 11, respectively.

It is clear from the results presented in Figs. 10 and 11 that the numerical solutions computed by using the SSPH, MLS and PD basis functions agree well with the analytical solution. Also, computed values 3.058, 3.032 and 2.971 of the stress concentration factor (SCF) at point O in Fig. 8b by using the SSPH, MLS and PD basis functions, respectively, differ from the analytical value 3.0 by less than 2%. The error norms, E_0^u for the u_2-displacement and E_0^σ for the σ_{11} stress defined by Eq. (4.8) for 369 particles, equal, respectively, 0.0303 and 0.0142 for the SSPH, 0.0118 and 0.0050 for the MLS, and 0.0234 and 0.0157 for the PD basis functions. When using the SSPH basis functions, the stress distributions computed with the three particle distributions converge to that for the analytical solution of the problem with an increase in the number of particles from 135 to 396 as shown in Fig. 12. One can conclude from the plot of strain energy error norm versus the minimum distance between adjacent particles that the rate of convergence for the strain energy equals 1.35, 1.36 and 1.43 for the PD, SSPH and MLS basis functions (Fig. 13).

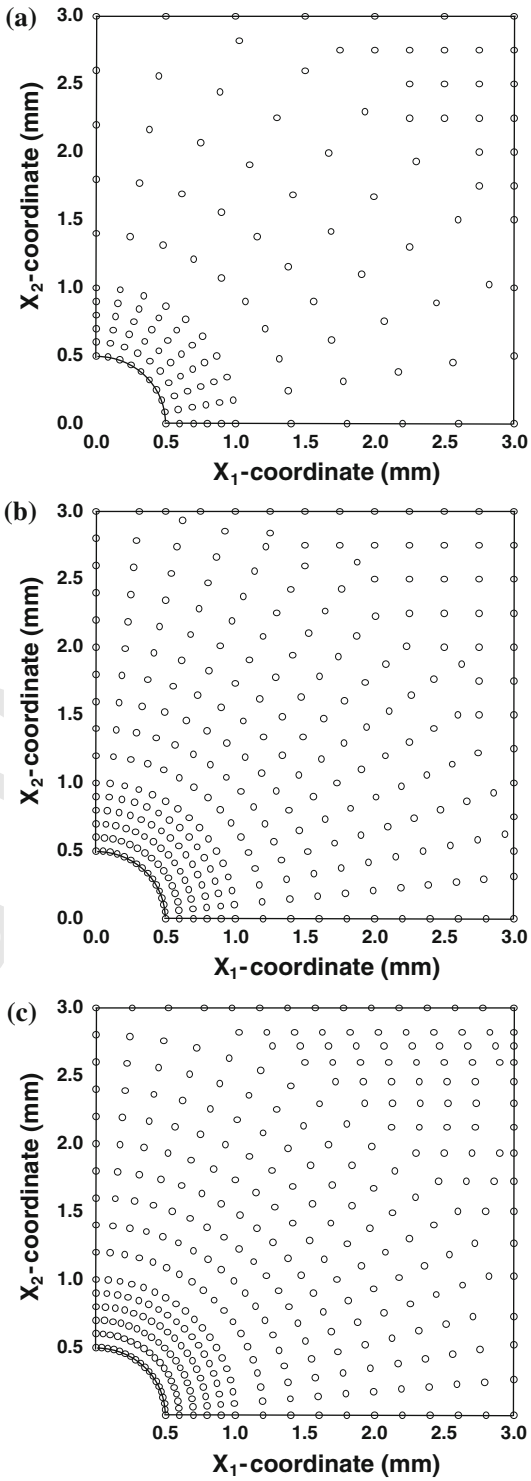

Fig. 9 Distribution of **a** 135, **b** 297, and **c** 369 particles in the domain

Journal: 466 MS: 0700 TYPESET DISK LE CP Disp.:2012/3/24 Pages: 16 Layout: Large

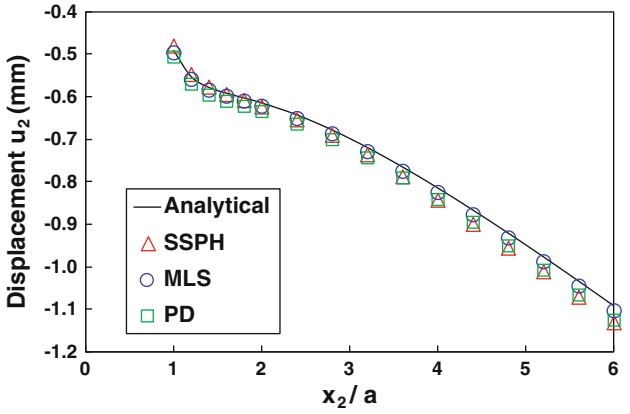

Fig. 10 Comparison of the analytical solution for the displacement u_2 along the x_2-axis with those computed by using the SSPH, MLS and PD basis functions (369 particles)

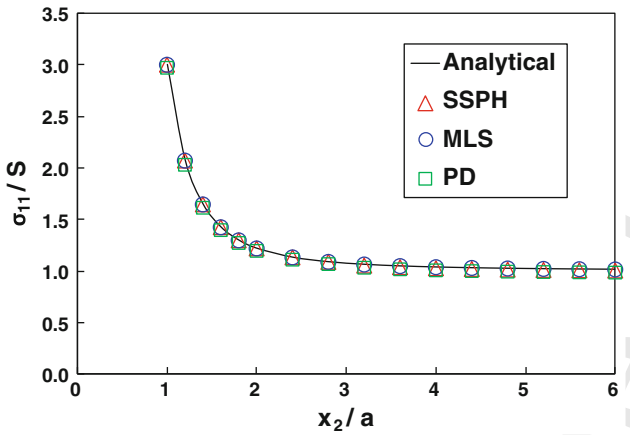

Fig. 11 Variation of the stress σ_{11} along the x_2-axis computed analytically and by using the SSPH, MLS and PD basis functions (369 particles)

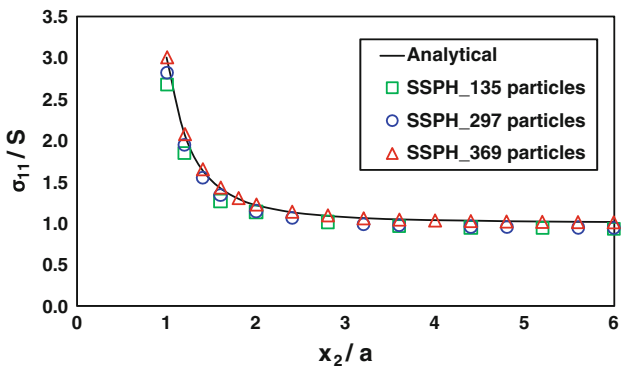

Fig. 12 Variation of the stress σ_{11} along the x_2-axis computed by using the SSPH basis functions and three distributions of particles

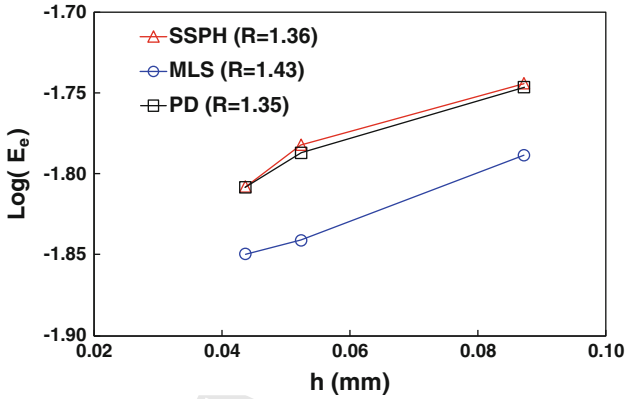

Fig. 13 Convergence of strain energy error norm and convergence rate, R, for SSPH, MLS and PD methods

5 Computational fracture mechanics

5.1 Plate with a crack at the center

We now study deformations of a rectangular plate with a crack symmetrically located at the plate centroid, as shown in Fig. 14a, and subjected to uniform tensile axial tractions at edges parallel to the crack face. The plate is made of a linear elastic, isotropic and homogeneous material. Values assigned to different parameters are H = 3.0 mm, B = 1.0 mm, E = 70GPa, υ = 0.3, and the half-crack length is varied from 0.1 to 0.8 mm. Because of the symmetry of the problem about the horizontal and the vertical centroidal axes, deformations of only a quarter of the plate in the first quadrant are analyzed. Fig. 14b depicts uniformly distributed particles in parts 1, 2 and 3 of the domain and the minimum distance between adjacent particles in these parts equals 0.025 mm, 0.05 mm and 0.1 mm, respectively. In order to capture the stress singularity near the crack tip, a refinement region, 0.1 mm × 0.1 mm, is placed around the crack tip and the distance between neighboring particles in the refinement region equals 0.005 mm. The stress intensity factor (SIF) is evaluated by using the interaction integral [19], $M^{(1,2)}$, given by

$$M^{(1,2)} = \int_\Gamma \left[W^{(1,2)}\delta_{1j} - \sigma_{ij}^{(1)}\frac{\partial u_i^{(2)}}{\partial x_1} - \sigma_{ij}^{(2)}\frac{\partial u_i^{(1)}}{\partial x_1} \right] n_j d\Gamma, \tag{5.1}$$

$$K_I = \frac{2}{E'} M^{(1,2)}, \tag{5.2}$$

where $W^{(1,2)} = \frac{1}{2}\left(\sigma_{ij}^{(1)}\varepsilon_{ij}^{(2)} + \sigma_{ij}^{(2)}\varepsilon_{ij}^{(1)}\right)$ is the mutual strain energy density, superscripts 1 and 2 in parentheses represent two different states of a cracked body. State 1, $(\sigma_{ij}^{(1)}, \varepsilon_{ij}^{(1)}, u_I^{(1)})$, corresponds to the present state and state 2, $(\sigma_{ij}^{(2)}, \varepsilon_{ij}^{(2)}, u_I^{(2)})$, is an auxiliary state chosen as the asymptotic

Journal: 466 MS: 0700 TYPESET DISK LE CP Disp.:2012/3/24 Pages: 16 Layout: Large

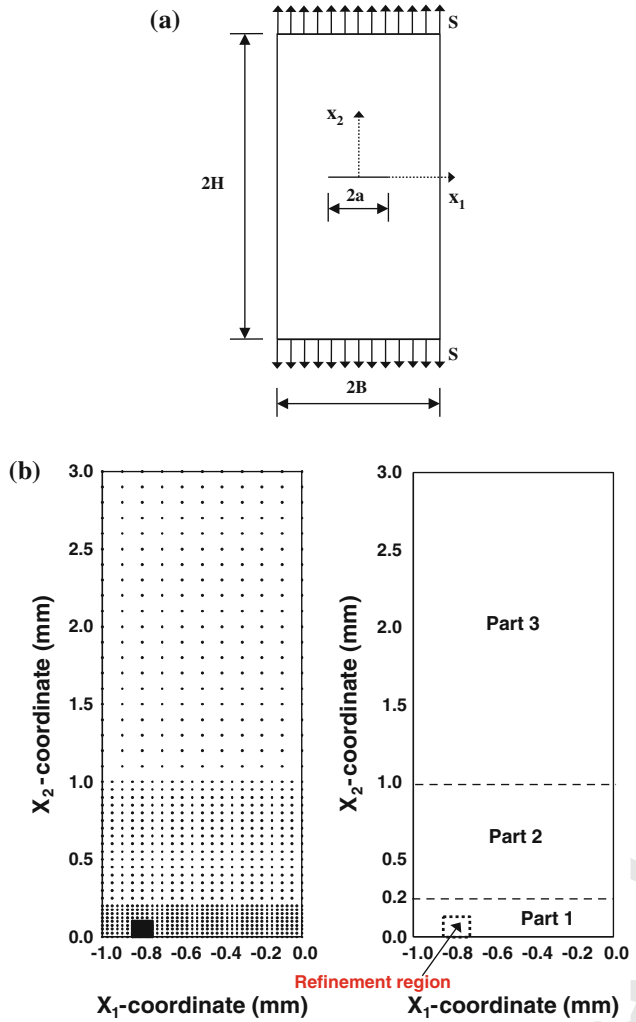

Fig. 14 **a** Specimen with a horizontal crack ($a/B = 0.2$), and **b** the distribution of particles in the quarter of the plate

fields for Mode I or Mode II. In Eq. (5.1) the contour Γ encloses the crack tip. For a finite-size plate, Aliabadi and L'opez [20] gave the following relation for finding the stress intensity factor (SIF) as a function of the crack length ratio r = a/B and the applied axial tensile stress S.

$$K_I = S\sqrt{\pi a}\left[1 + 0.043r + 0.491r^2 + 7.125r^3 - 28.403r^4 + 59.583r^5 - 65.278r^6 + 29.762r^7\right]. \quad (5.3)$$

In Table 5, we have compared the normalized values, $I = K_I/S\sqrt{\pi a}$, found from solutions of the problem obtained by using the MLS and the SSPH basis functions with that from Eq. (5.3). It is clear that both basis functions predict accurate values of I with the maximum percentage error of less than 2% even for a rather long crack.

Table 5 Normalized SIF, I, and the percentage error in I for the problem shown in Fig. 14

	a/B				
	0.1	0.2	0.4	0.6	0.8
I (SSPH)	1.0237	1.0692	1.2336	1.5038	2.0540
I (MLS)	1.0243	1.0673	1.2314	1.5026	2.0501
% Error (SSPH)	0.95	1.34	1.43	1.52	1.87
% Error (MLS)	1.01	1.16	1.25	1.43	1.68

5.2 Double edge notched (DEN) specimen

We now study deformations of a plate with two horizontal cracks emanating from opposite vertical edges and loaded by uniform axial tensile tractions S on the horizontal bounding surfaces parallel to the crack faces with the goal of determining the T-stress ahead of the crack tip; see Fig. 15a. Values assigned to different parameters are: H = 3.0 mm, B = 1.0 mm, the crack length ratio a/B = 0.2, E = 70GPa and $\upsilon = 0.3$. Because of the symmetry of the problem about the x_2-axis, deformations of only the left half of the plate are analyzed. The uniform distribution of particles is exhibited in Fig. 15b. The minimum distance between particles in the refinement region, and parts 1, 2 and 3 of the domain is 0.005 mm, 0.025 mm, 0.05 mm and 0.1 mm, respectively.

In cylindrical coordinates (r, θ) with the origin at the crack tip, the stress field around the crack tip can be expressed [21] as

$$\begin{bmatrix}\sigma_{11} & \sigma_{12}\\ \sigma_{12} & \sigma_{22}\end{bmatrix} = \frac{K_I}{\sqrt{2\pi r}}\cos\frac{\theta}{2} \times \begin{bmatrix} 1-\sin\left(\frac{\theta}{2}\right)\sin\left(\frac{3\theta}{2}\right) & \sin\left(\frac{\theta}{2}\right)\sin\left(\frac{3\theta}{2}\right)\\ \sin\left(\frac{\theta}{2}\right)\sin\left(\frac{3\theta}{2}\right) & 1+\sin\left(\frac{\theta}{2}\right)\sin\left(\frac{3\theta}{2}\right)\end{bmatrix} + \begin{bmatrix} T & 0\\ 0 & 0\end{bmatrix} + O\left(\sqrt{r}\right), \quad (5.10)$$

where T is the T- stress along the crack tip. Setting $\theta = 0$ in Eq. (5.10) gives

$$T = \sigma_{11}(r, 0) - \sigma_{22}(r, 0). \quad (5.11)$$

Values of T/S at r= 0.005 mm found from solutions of the problem by using the SSPH and the MLS basis functions for different crack length ratios, a/B, compare well with those obtained by Kfouri [22] as shown in Fig. 16.

6 Comparison with test results for crack propagation

We now study crack propagation in the double cantilever poly-methyl-metha-acrylate (PMMA) beam specimen exhibited in Fig. 17a with the ratio of the specimen height

Journal: 466 MS: 0700 TYPESET DISK LE CP Disp.:2012/3/24 Pages: 16 Layout: Large

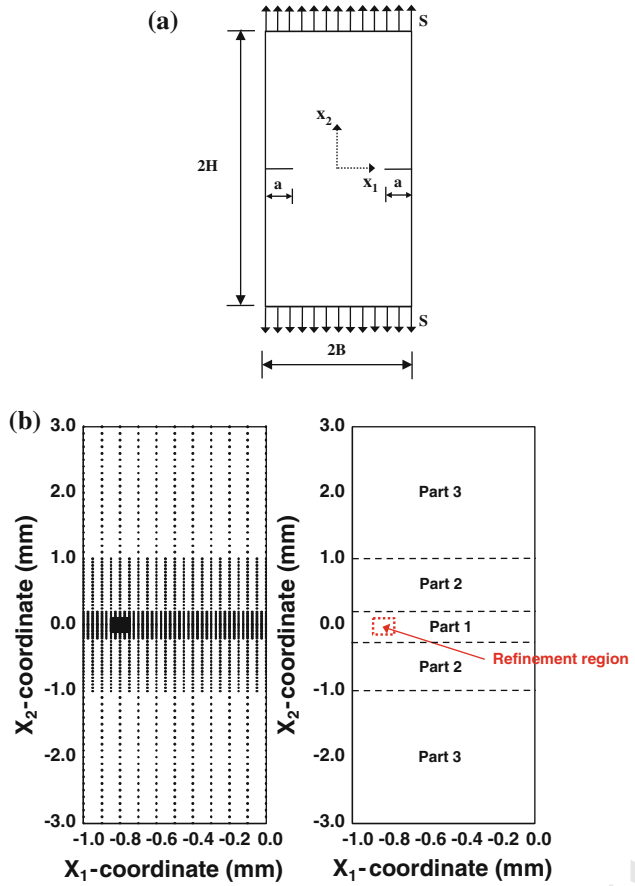

Fig. 15 **a** Double edge notched specimen ($a/B = 0.2$), and **b** the distribution of particles in the left half of the plate

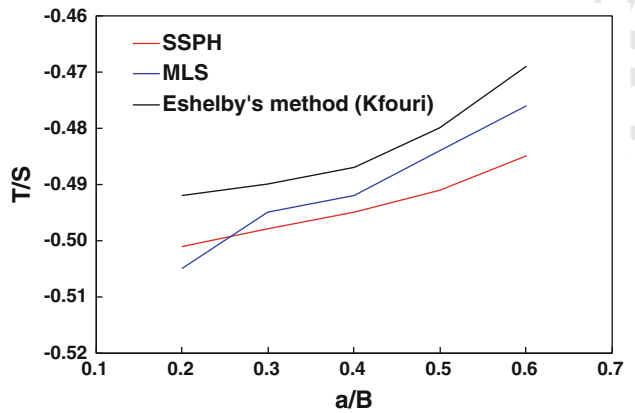

Fig. 16 Comparison of the values, T/σ, with the ratio, a/B, computed by using the MLS and SSPH basis functions

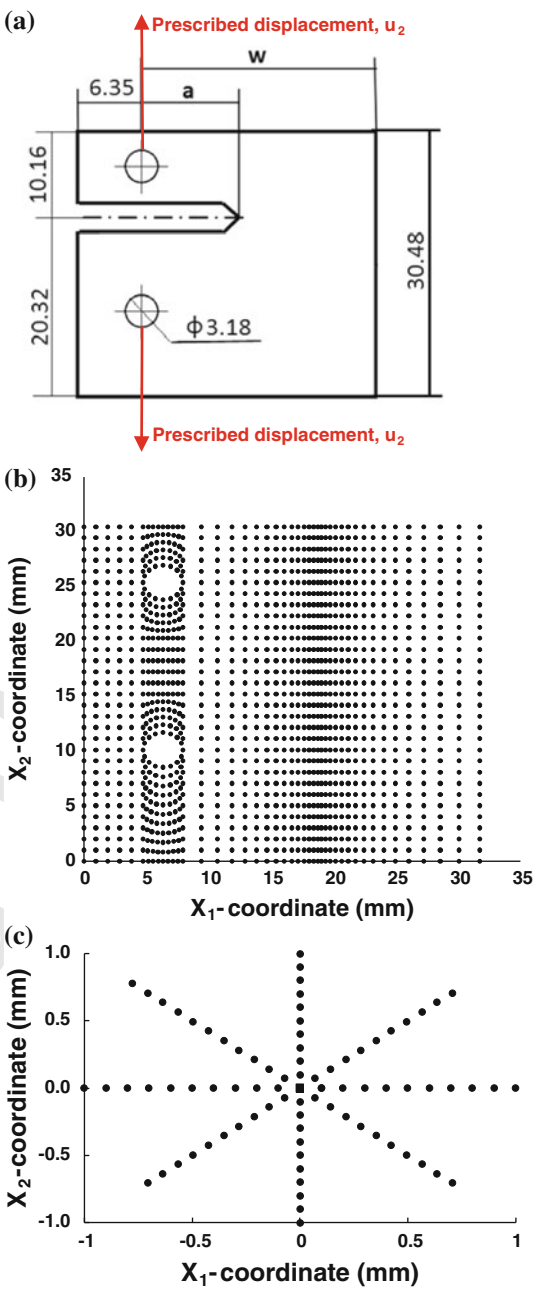

Fig. 17 **a** PMMA specimen asymmetric about the notch axis with $w = 25.4\,\text{mm}\ (1'')$, $a = 12.7\,\text{mm}\ (0.5'')$, and the ratio of the specimen height above the notch to that below it equal to 2. (All dimensions in mm); **b** the particles distribution; **c** particles distribution near the crack tip

above the notch to that below it equal to 2. Values assigned to material parameters are: E = 3.10 GPa and $\upsilon = 0.3$. Fig. 17b displays the layout of the particles. Additional particles, shown in Fig. 17c, are added around the crack tip to increase the accuracy of the computed SIF. As the crack propagates, these additional particles are moved with the advancing crack tip.

The SSPH and the MLS basis functions provide a smooth approximation of a function and of its spatial derivatives. However, the displacement field is discontinuous across a crack. The visibility criterion proposed by Belytschko et al. [13] is used to simulate the discontinuity in displacements by treating the crack as an opaque surface. When the domain

Journal: 466 MS: 0700 TYPESET DISK LE CP Disp.:2012/3/24 Pages: 16 Layout: Large

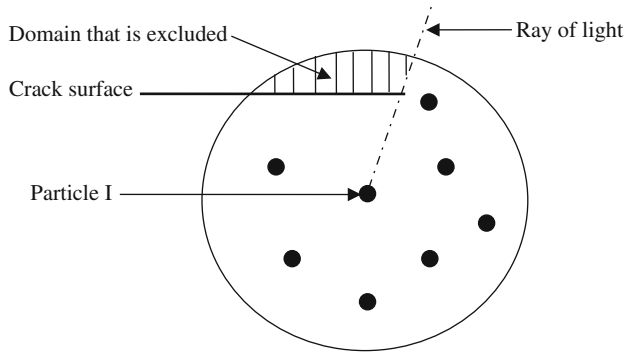

Fig. 18 Domain of influence of particle I by the visibility criterion

of influence for the weight function is constructed, the line from a point to a particle of interest is imagined as a ray of light. If the ray encounters the opaque surface, such as the crack surface, it is terminated and the point is not included in the domain of influence. Figure 18 shows the domain of influence of particle I near the crack tip and the domain that is excluded.

Plane strain deformations of the specimen are analyzed by using the two sets of basis functions and adopting the failure criterion proposed by Erdogan [23], i.e., the crack begins to propagate in the direction θ_0 for which the hoop stress reaches a material dependent critical value. In cylindrical coordinates with the origin at the crack tip, stresses at a point near the crack tip are given by

$$\sigma_{rr} = \frac{1}{\sqrt{2\pi r}}\cos\frac{\theta}{2}\left[K_I(1+\sin^2\frac{\theta}{2}) + K_{II}(\frac{3}{2}\sin\theta - 2\tan\frac{\theta}{2})\right] + T\cos^2\theta,$$

$$\sigma_{\theta\theta} = \frac{1}{\sqrt{2\pi r}}\cos\frac{\theta}{2}\left[K_I\cos^2\frac{\theta}{2} - \frac{3}{2}K_{II}\sin\theta\right] + T\sin^2\theta,$$

$$\sigma_{r\theta} = \frac{1}{\sqrt{2\pi r}}\cos\frac{\theta}{2}\left[K_I\sin\theta + K_{II}(3\cos\theta - 1)\right] + T\sin^2\theta, \quad (6.1)$$

where K_I and K_{II} are the mode I and the mode II stress intensity factors, respectively, and T is the non-singular axial stress ahead of the crack tip. The crack propagation angle θ_0 is found from

$$\frac{\partial\sigma_{\theta\theta}}{\partial\theta} = 0 \Rightarrow \theta = \theta_0,$$

or equivalently from (recall Eq. $(6.1)_2$)

$$\left[K_I\sin\theta_0 + K_{II}(3\cos\theta_0 - 1)\right] - \frac{16T\sqrt{2\pi r_c}}{3}\sin\frac{\theta_0}{2}\cos\theta_0 = 0, \quad (6.2)$$

where the critical distance r_c from the crack tip is taken to be r_c/a= 0.02. Once the position of the point (r_c, θ_0) has been ascertained, we substitute for r_c and θ_0 in Eq. $(6.1)_2$ and arrive at

$$\sqrt{2\pi r_c}(\sigma_{\theta\theta})_c = \cos\frac{\theta_0}{2}\left[K_I\cos^2\frac{\theta_0}{2} - \frac{3}{2}K_{II}\sin\theta_0\right] + T\sin^2\theta_0, \quad (6.3)$$

where $(\sigma_{\theta\theta})_c$ is the critical value of the tangential (or the hoop) stress at the critical distance r_c.

For pure mode I failure, the angle θ_0 in Eq. (6.3) equal zero; thus the critical value $(\sigma_{\theta\theta})_c$ is given by

$$\sqrt{2\pi r_c}(\sigma_{\theta\theta})_c = K_{Ic}, \quad (6.4)$$

where K_{Ic} is the material fracture toughness. Knowing the experimental value [24] of K_{Ic} (=1.056 MPa$\sqrt{m}$ for the PMMA) we get the value of $(\sigma_{\theta\theta})_c$ when a crack initiates.

The crack propagation analysis involves the following steps:

Step 1. The stress and strain fields are analyzed by using the meshless method.
Step 2. The angle θ_0 for which $\sigma_{\theta\theta}$ is maximum at r_c/a = 0.02 is found.
Step 3. If $(\sigma_{\theta\theta})_{max} < (\sigma_{\theta\theta})_c$, increase the applied vertical displacement until $(\sigma_{\theta\theta})_{max} = (\sigma_{\theta\theta})_c$.
Step 4. The crack is assumed to propagate when $(\sigma_{\theta\theta})_{max} = (\sigma_{\theta\theta})_c$ at $r_c/a = 0.02$ along the path making angle θ_0 with the x_1-axis.
Step 5. The crack is advanced through the critical distance, r_c.
Step 6. Move additional particles from the old crack tip to the new crack tip.
Step 7. Steps1 through 6 are repeated until the crack is fully developed.

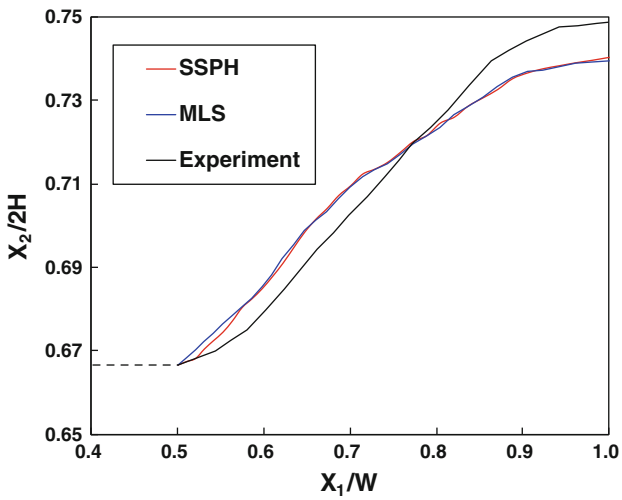

Fig. 19 Comparison of the computed crack trajectories from the SSPH and the MLS basis functions with the average experimental one for the asymmetric compact tension specimen of Fig. 17a

Journal: 466 MS: 0700 TYPESET DISK LE CP Disp.:2012/3/24 Pages: 16 Layout: Large

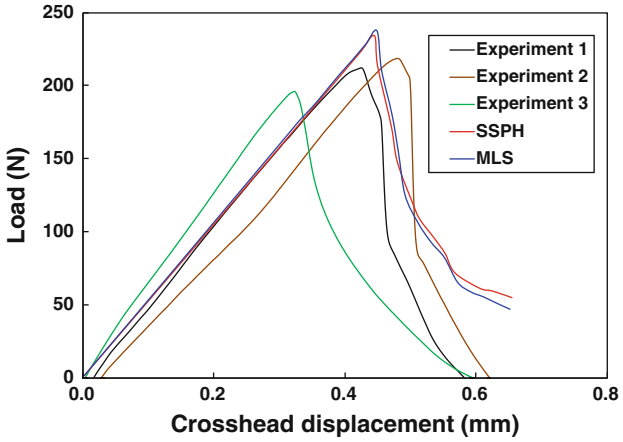

Fig. 20 For different values of the crosshead displacement, comparison of the computed load from the SSPH and the MLS basis functions with the experimental data for the asymmetric compact tension specimen of Fig. 17a

Figures 19 and 20 show a comparison of the predicted crack paths and the axial force vs. the crosshead displacement from the SSPH and the MLS basis functions with the experimental ones. It is clear that the predicted crack trajectories and the load obtained from both methods are in good agreement with the experimental results [24].

7 Remarks

In Sects. 4 and 5 we have verified the software by comparing the computed solution for several BVPs with their analytical solutions. Alternatively, one could use the method of manufactured solutions, e.g., see the material after Eq. (20) of [27] to verify the software.

We note that crack propagation in a linear elastodynamic problem using the SSPH basis functions has been studied in [28].

8 Conclusions

We have used basis functions derived by the moving least squares (MLS), the smoothed symmetric particle hydrodynamics (SSPH), and the pseudo-derivatives methods to analyze two dimensional elastostatics problems and compared these solutions with those obtained by employing either analytical or experimental techniques. The SSPH method has an advantage over the other two methods because basis functions used to approximate the function and its derivatives are derived simultaneously, and do not involve derivatives of the weight function. Thus piece-wise constant weight or kernel functions can be used to deduce the SSPH basis functions. The CPU time required to derive the SSPH basis functions is less than that needed to deduce the MLS basis functions. However, for the same particle distribution, results compared with the MLS basis functions have less error than that in results from the SSPH basis functions. The rate of convergence for the energy norm for the SSPH and the PD basis functions are nearly the same and a little better than that for the MLS basis functions.

By conducting numerical experiments with the bending of the beam problem and comparing the computed solutions with the analytical one, we have found optimal values of parameters for the weight function, the size of the compact support, and the order of the complete polynomials. It is found that the Gauss weight function and the radius of the compact support of the weight function associated with a particle equal to four times the smallest distance of the particle from its nearest neighbors provide better results than those with other choices of these variables. A good compromise between the accuracy of the computed solution and the computational cost is to use complete polynomials of degree two to generate the MLS and the SSPH basis functions.

We have also analyzed the stress concentration around a circular hole and the stress singularity at a crack tip in a plate deformed in plane strain tension and shown that the three basis functions successfully predict the stress concentration around the hole and the stress intensity factor at a crack tip. The crack paths in an asymmetric prenotched specimen loaded in tension predicted by using the SSPH and the MLS basis functions are found to agree well with that observed experimentally.

Acknowledgements This work was supported by National Science Foundation (NSF/CMMI Award No. 0826143) to Virginia Polytechnic Institute and State University.

References

1. Lucy LB (1977) A numerical approach to the testing of the fission hypothesis. Astron J 82:1013–1024
2. Lancaster P, Salkauskas K (1981) Surfaces generated by moving least squares methods. Math Comput 37:252–258
3. Liu WK, Jun S, Zhang YF (1995) Reproducing kernel particle methods. Int J Numer Methods Fluids 20:1081–1106
4. Hardy RL. (1990) Theory and applications of multiquadric-Biharmonic method. Comput Math Appl 19:163–208
5. Babuska I, Melenk JM (1997) The partition of unity method. Int J Numer Methods Eng 40:727–758
6. Zhang GM, Batra RC (2004) Modified smoothed particle hydrodynamics method and its application to transient problems. Comput Mech 34:137–146
7. Batra RC, Zhang GM (2004) Analysis of adiabatic shear bands in elasto-thermo-viscoplastic materials by modified smoothed particle hydrodynamics (MSPH) method. J Comput Phys 201:172–190
8. Batra RC, Zhang GM (2008) SSPH basis functions for meshless methods and comparison of solutions with strong and weak formulations. Comput Mech 41:527–545

Journal: 466 MS: 0700 TYPESET DISK LE CP Disp.:2012/3/24 Pages: 16 Layout: Large

9. Zhang GM, Batra RC (2009) Symmetric smoothed particle hydrodynamics (SSPH) method and its application to elastic problems. Comput Mech 43:321–340
10. Krongauz Y, Belytschko T (1997) Consistent pseudo-derivatives in meshless methods. J Comput Methods Appl Mech Eng 146:371–386
11. Liu GR (2009) Mesh free methods: moving beyond the finite element method. CRC Press, Boca Raton
12. Atluri SN (2005) Methods of computer modeling in engineering and the sciences. Tech Science Press, Palmdale
13. Belytschko T, Lu YY, Gu L (1994) Element-free Galerkin methods. Int J Numer Methods Eng 37:229–256
14. Ching H K, Batra RC (2001) Determination of crack tip fields in linear elastostatics by the meshless local Petrov-Galerkin (MLPG) method. Comput Model Eng Sci 22:273–289
15. Timoshenko SP, Goodier JN (1970) Theory of elasticity, 3rd edn. McGraw-Hill, New York
16. Monaghan JJ (1992) Smoothed particle hydrodynamics. Ann Rev Astron Astrophys 30:543–574
17. Belytschko T, Krongauz Y, Organ D, Fleming M, Krysl P (1996) Meshless methods: an overview and recent developments. Comput Methods Appl Mech Eng 139:3–47
18. Gingold RA, Monaghan JJ (1982) Kernel estimates as a basis for particle methods. J Comput Phys 46:429–453
19. Shepard D (1968) A two dimensional function for irregularly space data. In: ACM National Conference
20. Aliabadi MH, L/opez MH (1996) Database of stress intensity factors. Computational Mechanics Publications, Southampton
21. Shih CF, Asaro RJ (1988) Elastic-plastic analysis of cracks on bimaterial interfaces: part I—small scale yielding. J Appl Mech 55:299–316
22. Kfouri AP (1986) Some evaluations of elastic T-term using Eshelby's method. Int J Fract 30:301–315
23. Erdogan F, Sih GC (1963) On the crack extension in Constraint Effects in plates under plane loading and transverse shear. ASME 85:525–527
24. Tsai CL, Guan YL, Batra RC, Ohanehi DC, Dillard JG, Nicoli E and David DA (2010) Coupled experimental and computational analysis of fracture path selection in PMMA blocks. In: Proceedings society for experimental mechanics conference, June 2010
25. Liu GR, Gu YT (2005) An introduction to meshfree methods and their programming. Springer, New York
26. Willams ML (1957) On the stress distribution at the base of a stationary crack. J Appl Mech 24:109–114
27. Batra RC, Liang XQ (1997) Finite dynamic deformations of smart structures Comput Mech 20:427–438
28. Batra RC, Zhang GM (2007) Search algorithm, and simulation of elestrodynamic crack propagation by modified smoothed particle hydrodynamics (MSPH) method. Comput Mech 40: 531–546

Journal: **466** MS: **0700** ☐ TYPESET ☐ DISK ☐ LE ☐ CP Disp.:**2012/3/24** Pages: **16** Layout: **Large**